Colloids and Surfaces A: Physicochemical and Engineering Aspects 673 (2023) 131792

Contents lists available at ScienceDirect

Colloids and Surfaces A: Physicochemical and Engineering Aspects

journal homepage: www.elsevier.com/locate/colsurfa

Spreading dynamics on lithium niobate: An example of an intrinsically charged ferroelectric surface

Sushmitha Vinikumar, Clarissa Schönecker *

Institute for Micro Fluid Mechanics, Rheinland-Pfälzische Technische Universität Kaiserslautern-Landau, 67663 Kaiserslautern, Germany

GRAPHICAL ABSTRACT

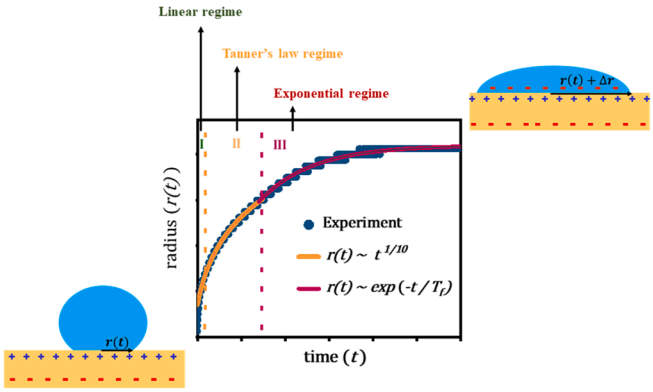

ARTICLE INFO

Keywords:
Lithium niobate
Charged surface
Droplet spreading
Wetting
Ferroelectric
Adsorption

ABSTRACT

Droplet wetting and manipulation are essential for the efficient functioning of many applications, ranging from microfluidic applications to electronic devices, agriculture, medical diagnosis, etc. As a means of manipulating droplet wetting, the effect of applying an external voltage or surface charge has been extensively exploited and is known as electrowetting. However, there also exist many materials which bear a quasi-permanent surface charge, like electrets, which are widely employed in sensors or energy storage. In addition, other materials in nature can acquire surface charge by the triboelectric effect, like human hair, natural rubber, and polymers. Nevertheless, there do not exist any studies on spreading on this class of charged surfaces. In our work, we for the first time investigate spreading dynamics on lithium niobate ($LiNbO_3$) as an example of a ferroelectric material with strong instantaneous polarization ($0.7\ C/m^2$). We find a spreading behavior that significantly differs from classic surfaces. Spreading times can be significantly enlarged compared to standard surfaces, up to hundreds of seconds. Furthermore, the classic Tanner's law does not describe the spreading dynamics. Instead, the evolution of the droplet radius is dominated by an exponential law. Contact angles and spreading dynamics are also polarization-dependent. They are also influenced by adsorption layers, such as they are left behind by cleaning. Overall, all results indicate that adsorption layers play a significant role in the wetting dynamics of lithium niobate and possibly other charged materials, where such processes are very pronounced. Possible mechanisms are discussed. Our findings are essential for the understanding of wetting on charged surfaces like ferroelectric

* Corresponding author.
E-mail address: c.schoenecker@rptu.de (C. Schönecker).

https://doi.org/10.1016/j.colsurfa.2023.131792
Received 17 March 2023; Received in revised form 30 May 2023; Accepted 31 May 2023
Available online 1 June 2023

materials in general. The knowledge of surface charge-based wettability difference, surface charge specific adsorption and its impact on wettability can be utilized in applications like, printing, microfluidics, triboelectric nanogenerators, and to develop biocompatible components for tissue engineering.

1. Introduction

Understanding and control of surface wettability is crucial in many applications like inkjet-based printing [1,2], electronic displays [3,4], self-cleaning surfaces [5], electrocatalysis [6,7], but also in medical applications like lab-on-a-chip application [8–10] and diagnostics [9,11, 12]. Wettability depends on various parameters, like surface and fluid chemistry, surface roughness, adsorption, intermolecular forces, etc. Also, the surface charge is an important parameter that affects the wetting dynamics [13]. The surface charge can originate from various sources. It can be naturally present, as in the case of ferroelectrics, or artificially induced, as in the case of certain classes of electrets. Furthermore, materials can acquire surface charge, for example, from triboelectric charging [14,15] or external polarization [16]. In triboelectric charging, after frictional contact between two materials, materials gain opposite charges [17,18]. This applies to materials like human hair or natural rubber, many inorganic materials, and polymers, which are a widely used class of material in the industry and daily life applications. In addition, adsorption on the surface may lead to surface charges [19].

Semiconductor and ferroelectric materials have gained tremendous importance in recent years, as they are widely applied in harvesting and scavenging energy [20]. For these purposes, understanding charge transfer between dielectric materials contacting fluids is of utmost importance. In particular, during recent years, triboelectric nanogenerators (TENG) have been widely investigated for their ability to efficiently convert mechanical energy into electric power (for as review, see, [21]). One particular type of TENGs is based on the principle of droplets sliding down a surface [22–30]. Thereby, both the surface as well as the droplet become electrified [23–27]. Such processes similarly occur for raindrops or flowing water. For the charging of the droplets, electric double layers that form at the solid-liquid interface are an integral part of the process. Because the droplet is moving, also the relation between the characteristic times for charge distribution within the droplet vs droplet motion are important.

In general, electric effects have been widely used to modify the contact angle of droplets sitting on dielectric surfaces via electrowetting. Here, an external electric field is applied to the droplet via specific electrode arrangements. Electrowetting has demonstrated significant changes in the contact angles of droplets. Yet, even without an external electric field as in electrowetting, the mere presence of an electric double layer at a surface has been theoretically calculated to lead to a modification of the static contact angle of the droplet deposited on the surface [31].

For intrinsically charged surfaces like ferroelectric materials, the difference to the aforementioned scenarios is that electric charges exist a priori everywhere on the surface. They do not only develop after contact with the fluid of the droplet or after an external trigger but are present both at the solid-liquid interface underneath the droplet as well as at the solid-gas interface next to the droplet (cf. Fig. 1).

Surface charges were also theoretically calculated to modify the spreading dynamics [31]. For the above-mentioned classes of materials, a specific spreading behavior influenced by surface charges is hence conceivable.

Due to their permanent surface charge, ferroelectric materials are therefore an interesting class of materials to be investigated for their interaction with water droplets. This applies both to fundamental aspects, such as to which extent spreading or sliding may differ from uncharged surfaces, as well as with respect to possible applications, as in TENGs. Within this class of materials, lithium niobate (LN) is especially remarkable, as it possesses one of the largest known surface polarizations (about $0.7\ C/m^2$).

Despite having enormous applications, little knowledge is available on the wetting behavior of LN. Wavelength-dependent reversible wettability was investigated on *z*-cut surface; the wettability of the LN wafer can be increased using UV light irradiation and restored with IR radiation irradiation [32]. The impact of heating on the wettability of *z*-cut lithium niobate was studied on LN using ionic liquids. In these studies, the contact angle decreased after the heat treatment [33]. Al-Shammari et al. demonstrated the wettability modification of LN surface using metallic nanostructure deposition [34]. Since all these studies focused on static conditions, there is however no information available on the dynamics of wetting on LN.

In this work, we, therefore, investigate the spreading dynamics on the widely used ferroelectric material lithium niobate (LN) and compare them with classic spreading dynamics.

1.1. Lithium niobate

Lithium niobate ($LiNbO_3$) is an artificially grown, dielectric, single crystal; it is ferroelectric, pyroelectric, and piezoelectric. It is widely used in nonlinear optics and electro-optic applications [35], catalyst [36,37], metasurface [38], sensors [39,40], integrated electronics [41] microelectrochemical systems [42], thermal infrared detectors [43,44], MEMS power generator [45], opto-microfluidic sensing [46], as electrode material in lithium-ion batteries [37], Memory units [47], and neuromorphic systems [48]. LN's unique polarization behavior and biocompatibility make it a desirable material for biocompatible

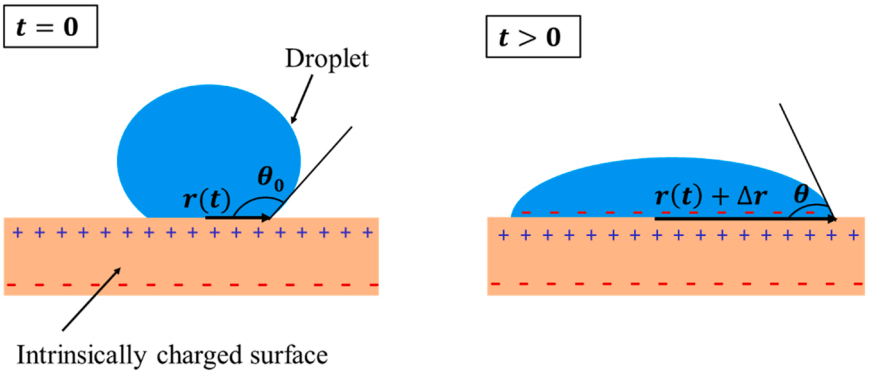

Fig. 1. Schematic of water droplet sitting on a poled intrinsically charged surface.

components for tissue engineering [49,50]. The ability of LN to switch polarization from external stimuli is explored in investigating charge based control of cell adhesion and cellular interactions [51].

LN atoms arrange in unit cells as depicted in Fig. 2. The LN structure above the Curie temperature consists of LiO_3 and Nb sheets piled along the z-axis, The Nb^{5+} and Li^{+} atoms [52] are centered between oxygen layers, and the material is nonpolar (Fig. 2, paraelectric phase). Below Curie temperature, the elastic force in the crystal dominates and forces Nb^{5+} and Li^{+} ions to leave their positions [52]. The charge separation resulting from the shift makes the material polar. (cf. Fig. 2, ferroelectric phase).

In the case of unpoled LN crystal, the domains are randomly oriented. A poling process aligns the randomly oriented ferroelectric domains in the crystal to orient along z-direction. Poled $z-cut$ is obtained by heating the crystal above the Curie temperature ($1142°C$) and applying an electric field along the z-direction. The spontaneous polarization is relatively high along the z-axis [53,54]. Cutting the material perpendicular to this direction yields z-cut [52,55] with two differently polarized surfaces: positive((0001)or $+z$-cut) and negative ($(000\bar{1})$or $-z$-cut). A theoretical study based on density functional theory conducted by Levchenko et al. and S. Sanna et al. predicts the most stable termination for LN $+$z-cut side is Nb-O_3-Li_2, and the $-z$-cut side is O-Li [52,56]. Molecule-surface interactions depend on surface charge, which in turn depends on polarization direction, surface termination, and the crystal plane.

LN possesses one of the largest known spontaneous polarizations of about $0.7\ C/m^2$ along the z-axis [52,55,57–59]. Due to this large surface charge, LN is a widely studied material in Kelvin probe force microscopy (KPFM) [60–62]. It has been shown that under atmospheric conditions, the surface charge causes the adsorption of screening charges from the air [63,64]. In KPFM under atmospheric conditions, the magnitude of surface potential perceived by the cantilever depends on this screening layer, which mainly consists of water [17,63,64].

2. Materials and methods

For the experiments, poled and double-side polished z-cut LN wafers (G and H Photonics, thickness 0.5 mm) were employed. Contact angles and spreading dynamics of a water drop deposited on an LN surface were observed using a Krüss DSA30 drop shape analyzer. The experiments were performed inside a humidity chamber, with a controlled temperature of $25°\ C$ and relative humidity (RH) of 50%. These conditions correspond to typical environmental conditions as they could for example occur for droplets moving on a substrate or for small-scale fluid-based tribogenerators. They are stable over the entire duration of the experiments. For the control of the environmental conditions, a humidity chamber (Krüss HC10) and an environmental chamber (Krüss TC30) were employed. The temperature in the environmental chamber was heated and maintained via a thermostat fluid circulation (IKA @HRC 2 basic). Humidity was controlled via the Advance software of the Krüss DSA30. The needle was grounded with a copper wire to protect the experiment from potential charge interference. The water droplet (ultrapure water: SG Ultra Clear TWF / El-Ion UV plus TM resistivity 18.2 $M\Omega.cm$) was first dosed and formed a droplet hanging on the needle. It was then slowly lowered and deposited on the surface to reduce the effect of impact on the droplet dynamics. Droplet spreading on the surface was observed using the high-speed camera of Krüss DSA30 with 800 fps. Droplet spreading was studied for different positions of the wafer. The contact angle was evaluated on both sides of the wafer using the ellipse fitting method. For the evaluation of the spreading radius,

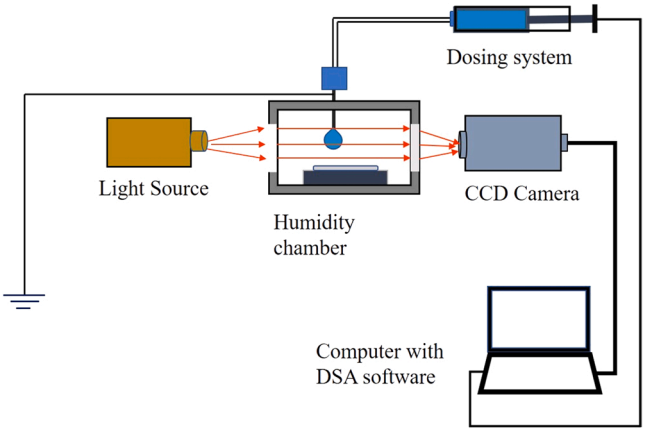

Fig. 3. Schematic diagram of the experimental setup: Krüss Drop Shape Analyser DSA30 with humidity and temperature chamber.

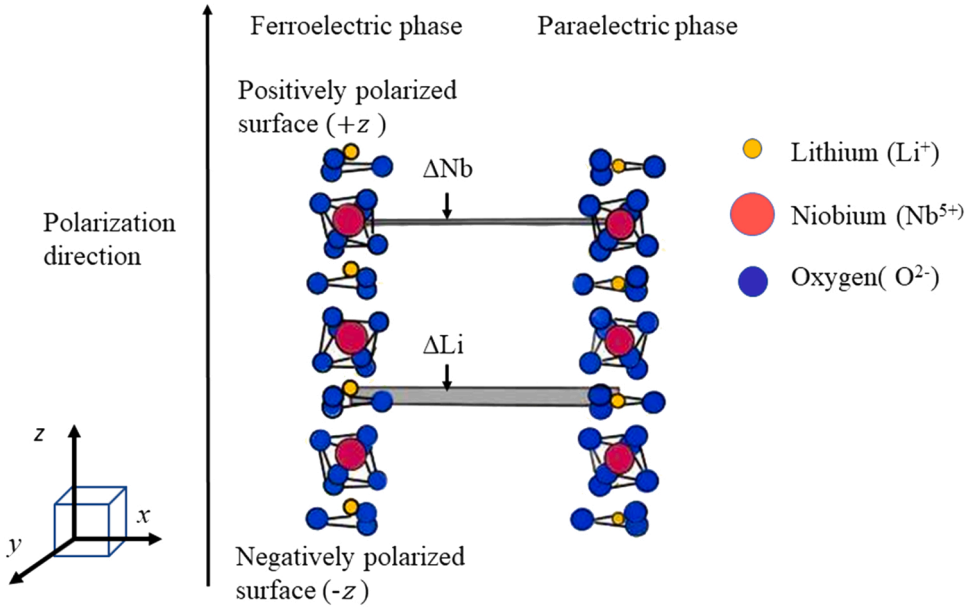

Fig. 2. Schematic diagram of an LN z-cut atomic model. ΔLi indicates the displacement of Li^{+} along the z-axis, ΔNb indicates the displacement of Nb^{5+} cations along the z-axis with respect to the oxygen plane.

Krüss Advance software was employed. Fig. 3.

Because the adsorption of moisture and contaminants from the air may be influential, a defined reference state of the surface is essential. In the standard case, wafers were cleaned using ultrasonication with acetone, ultrapure water, and isopropanol, respectively, for 10 min each. Wafers were dried immediately using clean room tissues to avoid any water mark formation. The wafers were stored in a desiccator containing desiccant to avoid any possible adsorption of impurities due to the high surface charge. Experiments were performed after 4 days of storage after ultrasonic cleaning to ensure a reproducible reference state.

Furthermore, to study the effect of adsorption on the spreading dynamics of the droplet, we let isopropanol (IPA) and ultrapure water adsorb to the surface. For this, the dryly stored LN wafer was immersed in the adsorbate liquid for 5 min, and the excess liquid was removed with a clean room tissue. Measurements of the contact angle were made, and the droplet's spreading dynamics were studied, as previously mentioned.

To compare the spreading dynamics of LN, materials with similar contact angles as LN were considered, namely PMMA and PVC, copper and aluminum. The metal surfaces were cleaned using ultrasonication as described above, and polymer surfaces were cleaned with ultrapure water. Surfaces were stored in the desiccator.

For all experiments, a small droplet of 3 µl volume was used. The small droplet size ensured that the droplet was always below the capillary length (2.7 *mm* for water) so that gravitational forces should not play a role [65,66]. Correspondingly, the Bond number $Bo = \frac{g\rho L^2}{\gamma}$, which characterizes the relation of gravitational to capillary forces, was always $< <1$. Here, g is the gravitational acceleration, ρ the density of water ($1000\ kg/m^3$), L the characteristic length, i.e., the base radius of the droplet, and γ is the surface tension ($0.072\ N/m$).

3. Results and discussion

3.1. Dynamics of droplet spreading

In general, when a droplet is deposited on a surface, it spreads outwards until it achieves its equilibrium shape. Consistently, this behavior is also apparent for a water droplet on an LN surface. Yet, there are significant differences compared to classic spreading: Firstly, in the general spreading evolution, and secondly, in the time it takes for the droplet to reach its final radius.

3.1.1. General spreading behavior

The classic way to describe droplet spreading is Tanner's law. It relates the base radius of the droplet r to the time t by the power law $r(t) \sim t^n$, where n represents the wetting exponent. For the viscous spreading of small droplets, hydrodynamic theory predicts that the initial spreading is driven by capillary forces and opposed by the viscous dissipation at the wedge-like region near the contact line. In this case, $n = 1/10$. Tanner's law is not valid at very short times. When the droplet radius grows beyond the capillary length, gravity becomes influential ($n = 1/8$).

It is evident from Fig. 4(a) that Tanner's law alone does not adequately describe the experimentally measured spreading radius on LN. Despite there is, of course, a similar trend, Tanner's $1/10$ law partly over and underestimates the experimental data. Also, different wetting exponents from $n = 1/10$ are not able to yield an appropriate description of the spreading radius.

A theoretical model for electrolyte drop spreading on charged surfaces has been proposed by Sinha et al. [31]. This model considers the presence of an electric double layer. The study considers three regimes for the spreading of an electrolyte drop placed on a charged surface: I) An initial regime with a steep, linear increase of the base radius with time; II) an intermediate regime where Tanner's law is valid; III) a near-equilibrium regime, where the radius exponentially approaches its final value: $r(t) \sim r_{\text{equilibrium}} - \exp(-\frac{t}{T_f})$, with T_f being the characteristic time of this equilibrating process.

Indeed, the spreading behavior of a droplet deposited on a lithium niobate surface can be well described under the assumption of a I) a linear regime $r(t) \sim t$, II) a power law a regime $r(t) \sim t^{1/10}$, and III) an exponential regime (Fig. 4(b)).

While Sinha et al. [31] further divided the intermediate regime into two sub-regimes, with the first $r(t) \sim t^{1/7}$ under the assumption of dominating contact line dissipation, and later $r(t) \sim t^{1/10}$ for dominating bulk dissipation, we restrain the fit of the experimental data to $r(t) \sim t^{1/10}$, because the difference is practically small.

It is obvious that a simple Tanner's law description of the spreading is insufficient for lithium niobate. More detailed models have to be employed. It is necessary to include the more pronounced exponential regime.

The three regimes, I, II, and III are not explicitly predicted only for charged surfaces. They are already part of a general model for partial wetting dynamics by de Ruijter et al. [67]. However, in classic wetting, the focus is on Tanner's law, while the exponential regime is usually not considered. Sinha et al. [31] expanded de Ruijter's model to charged surfaces and calculated the specific influence of the presence of an

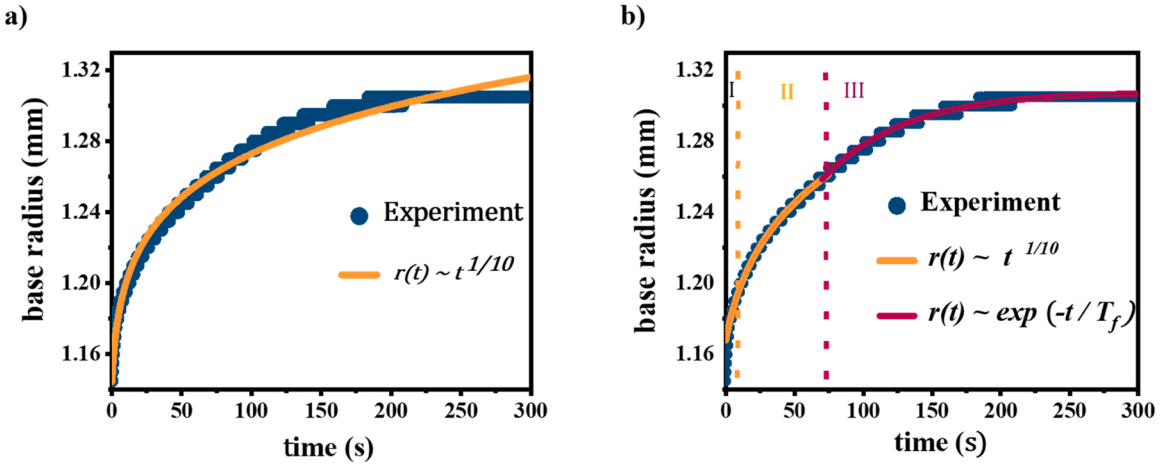

Fig. 4. (a) Measured base radius of a droplet spreading on an LN surface and inappropriate fit by the classic Tanner's law; (b) Dynamic spreading of a water droplet on an LN surface. The division into three regimes: I) linear $r(t) \sim t$, II) power law $r(t) \sim t^{1/10}$, III) exponential $r(t) \sim \exp(-t)$.

electric double layer to affect the prefactors and characteristic time scales that govern the onset and behavior throughout the three regimes [31]. For charged surfaces, the first regime is calculated to have a steeper increase in the base radius and short duration than for uncharged surfaces. Specifically, for the third regime, the timescale T_f is predicted to be enlarged, which the authors interpret as a later onset of the third regime for charged surfaces compared to uncharged surfaces [31].

3.1.2. Spreading times

It is remarkable that in the experiments, the spreading process takes place over very extended periods of time. The droplet spreads for about 50–200 s until it reaches its final diameter. This time is much longer than typical spreading times. Fig. 5 shows a comparison of the initial spreading behavior between LN and a variety of typical materials that possess a similar contact angle as LN (about 75–90°). Under the same environmental conditions, only droplets on the polymer PMMA require a few seconds to spread entirely, while on PVC, aluminum and copper no spreading could be visualized with a frame rate for data collection of 20 fps. To the eye, the droplets instantaneously adopted their final radius. In contrast, the spreading time on LN takes up to several orders of magnitude longer.

Classic theories are not able to explain these extended spreading times. One approach to estimating spreading times is the theory provided by Sinha et al. [31]. They present scaling relations for the impact of the electric double layer on the characteristic times for the duration t_1 of phase I and the timescale T_f of the exponential phase III:

$$t_1 = \frac{(\zeta_f + \eta)R_0}{\gamma \cos\theta'_{eq} \ln\left(\frac{3V}{2\pi a^3}\right)} \tag{1}$$

and

$$T_f = \frac{\eta R'_{eq}\left[\delta + \frac{8}{3\theta'_{eq}}\ln\left(\frac{3V}{\pi a^3(\theta'_{eq})}\right)\right]}{3\Upsilon\theta'^{2}_{eq}} \tag{2}$$

Here, η is the viscosity of the fluid, γ is the surface tension, V is the volume of the droplet, R_0 is the initial base radius of the droplet, R'_{eq} and θ'_{eq} are the equilibrium base radius and equilibrium contact angle (when the droplet attains the constant base radius phase) in the presence of an electric double layer. Here, a, δ and ζ_f are system-specific parameters related to dissipation. They were determined by de Ruijter et al. [67] for a droplet of di-n-butyl phthalate (DBP) on poly(ethylene terephthalate) (PET) substrate [68]. However, they are not known for the present system, so Eqs. (1) and (2) cannot be employed in the current situation. As a test, with the parameter of the present system (V=2.8 μl, R_0 =1.14 *mm*, R_{eq}=1.31 *mm*, θ'_{eq}=70°.) and de Ruiter's values for a, δ, and ξ_f, characteristic times of the order of milliseconds are obtained: $t_1 \sim 2.4 \times 10^{-4}$ s, $T_f \sim 1.44 \times 10^{-3}$ s. Hence, despite the fact that, T_f is enlarged by the presence of an electric double layer, these times cannot describe the very extended spreading time on LN. Besides the lack of parameter values, another possible reason for this discrepancy is that the electric double layer is assumed to be priorly present in the case of Sinha's calculations.

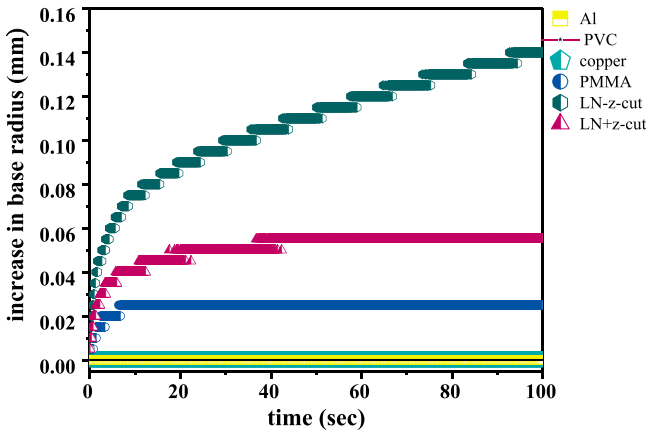

Fig. 5. Droplet spreading on different surfaces during the first 100 s at 25 °C and 50% RH. For PVC, copper and aluminium, spreading is not observed, so the data points lie on top of each other at 0.

Another approach to estimate spreading times stems from electrowetting. It is known from this field that not only the electric double layer has to build up, but also the whole droplet has to evolve to equilibrium with respect to the distribution of charges. This time can be modeled using equivalent electric circuit models [69–72]. Here, the droplet is described as a resistance R, while the electric double layer and the (under electrowetting conditions typical) dielectric layer between the droplet and the underlying electrode constitute a capacitor with capacitance C. The characteristic charging time of the capacitor within this circuit gives the typical spreading time after applying a voltage across the droplet.

$$\tau = R{\cdot}C. \tag{3}$$

The resistance of the droplet can be estimated by the resistance of a conductor $R \sim \rho L/A$, with ρ being the resistivity of the fluid, L it is the typical length, i.e., the droplet height, and A the base area. The capacitance is $C = \epsilon_0 \epsilon_r A/d$, with d being the distance between the capacitor plates. In the present case, only the capacitance of the double layer remains. With a typical height of the droplet of $L = 1$ *mm*, the resistivity of the ultrapure water $\rho = 18.2$ *MΩ.cm*, and the distance being of the order of the Debye length $d \sim \lambda_D \sim 100$ *nm*, the predicted spreading time is about $\tau \sim 1.2$ *s*.

This value is much closer to the experimentally observed times yet still up to one or two orders of magnitude smaller. Hence, neither an electrowetting analogy is able to describe the temporal evolution of droplet spreading on the electret lithium niobate. Apparently, even slower processes take place, as will also be discussed later.

Further influence factors on the contact angle and spreading times are investigated in the following.

3.2. Effect of polarization direction on spreading dynamics

The LN wafers possess two differently polarized sides according to their atomic arrangement (cf. Fig. 2). Time-dependent contact angles and spreading were studied on both sides.

In general, there is a significant difference of approximately 10° degrees between the contact angles of the two sides (Fig. 6(a)). This difference is in line with studies of Rusul M. Al-Shammari et al. [34], who found the negative side of z-cut LN to be less hydrophilic than the positive side by the same amount.

Regarding the dynamic behavior, we found that on the $-z$-cut, the spreading time is about a factor of 4 larger than on the $+z$-cut, cp Fig. 6 (b). Still, both times are much larger than a simple electrowetting estimation would suggest. As discussed above, the long spreading times are likely not a purely electrowetting-like effect. This is also supported by the fact that a simple electrowetting analogy would suggest that the side with the smaller contact angle possesses the larger charge. While this fact would not change the spreading time in an electrowetting analogy, according to Sinha et al. [31] this would result in a longer spreading time. This is the opposite of the observed behavior, suggesting that other processes might play a role.

One possible process is that the high surface charge leads to a significant but different amount of adsorption of water molecules (and possibly other species) from the surrounding air. It is reasonable to assume that more preexisting moisture on the surface would lead to a lower contact angle and faster spreading. Also, in the present data, the side with the lower contact angle shows the shorter spreading time. These circumstances will be further investigated in Section 3.3.

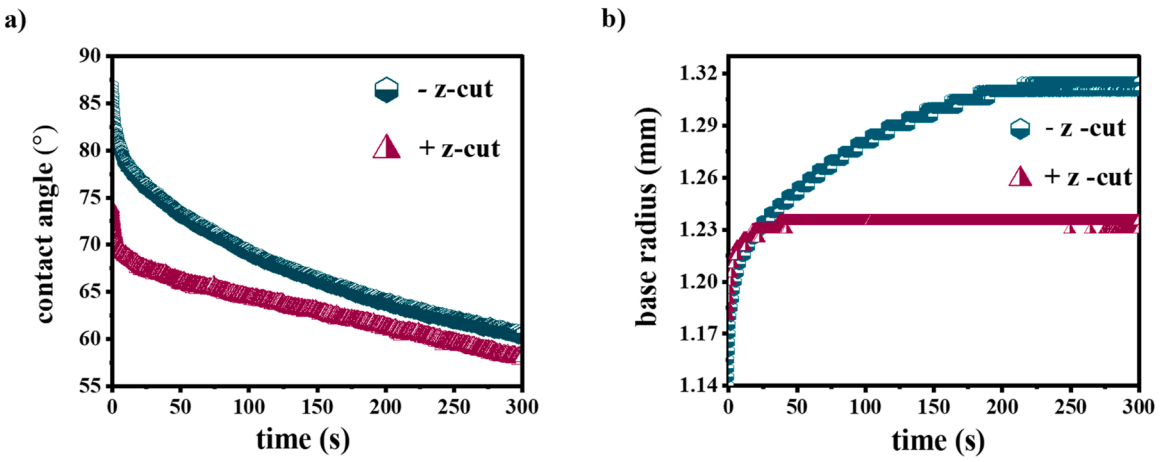

Fig. 6. (a) Time-dependent contact angle for − *z*-cut and +z-cut; (b) Radius evolution during droplet spreading on − *z*-cut and + *z*-cut.

Furthermore, despite the humidity and temperature control, substantial evaporation prevents the measurement of a static contact angle (Fig. 6(a)). However, the rate of change of the contact angle is smaller during the constant-radius phase than during the initial phase. Hence, even if there was a similar evaporation present during the initial phase as during the constant-radius phase (reflected in the rate of change during the constant-radius phase), this influence should not be dominating.

3.3. Impact of adsorption or cleaning on the spreading dynamics

As the surface charge of lithium niobate is known to lead to the adsorption of water molecules on the surfaces, moisture adsorbed to the surface could influence the spreading dynamics and contact angle. First, this is important as a general mechanism that influences spreading. Second, adsorption may be altered by cleaning processes employed prior to wetting measurements.

3.3.1. Short time influence of the cleaning procedure on the contact angle

In this work, the surfaces were cleaned by sequential ultrasonication in acetone, isopropanol, and water, and excess water is removed from the surface with a cleanroom tissue. To observe the effect of cleaning, individual droplets were placed on different places of an LN wafer at certain time intervals after cleaning. The contact angle immediately after cleaning is significantly reduced to about half the value for a surface kept in a desiccator for 4 days (Fig. 7, for a better overview, only the initial contact angles are shown). The contact angle for a freshly deposited droplet also changes notably with the time after cleaning. Within the first 30 min, it rose from a value of 34° to roughly 48°.

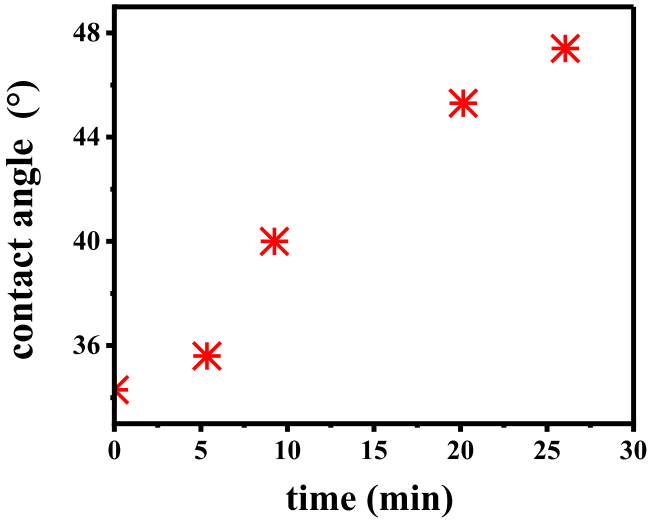

Fig. 7. Initial contact angles of individual droplets placed on an -*z*-cut LN surface at time *t* after cleaning and drying the wafer with clean room tissue.

This decrease in contact angle also illustrates the impact of cleaning in general when performing wetting studies. Consistently, Al-Shammari et al. [34], who investigated contact angles on LN *z*-cut surfaces that were not dryly stored after cleaning, reported lower values than ours from long-term storage.

The drastic change in the contact angle shows that there are significant processes going on at the surface. Apparently, these processes are related to adsorption. It is likely that there are remains of the cleaning liquid adsorbed to the surface. These adsorbates are in contact with the surrounding air. They obviously need large times to equilibrate to a stationary state.

3.3.2. Influence of the adsorbate liquid on the spreading dynamics

As indicated in the previous part, adsorption through cleaning is substantial. Regarding the spreading dynamics, we studied the impact of commonly used cleaning agents, water, and isopropanol.

Since the actual adsorption at the surface could not be measured under ambient conditions, we modified the amount of adsorbed liquid by immersing the LN in adsorbate liquid. After carefully removing the liquid left on the surface using a clean room tissue, the contact angle and radius of the droplet were evaluated for a given amount of time. It is expected that after immersion in the adsorbate liquid, the amount of adsorbed molecules increases, compared to a dryly stored wafer.

Both liquids alter the contact angle significantly (Fig. 8(a)). Isopropanol causes an even stronger contact angle decrease than water. At the same time, the spreading time is significantly lowered by the cleaning agents (Fig. 8(b)). Isopropanol-treated surfaces attain the equilibrium radius much faster compared to water-pretreated surfaces. It appears that the more the contact angle is lowered by adsorbents, the more the spreading time is shortened.

3.4. Discussion

Obviously, the spreading dynamics on lithium niobate differ from classic spreading behavior, especially with respect to the long spreading times until the droplet reaches its constant base radius. As classic theories, such as an electrowetting analogy, are not able to explain this behavior, other slower processes are apparently taking place. It is likely that these processes are connected to adsorption layers that form on the LN's surface. The high surface charge of LN is known to attract moisture and possibly other species from the surrounding air [47,73]. Hence,

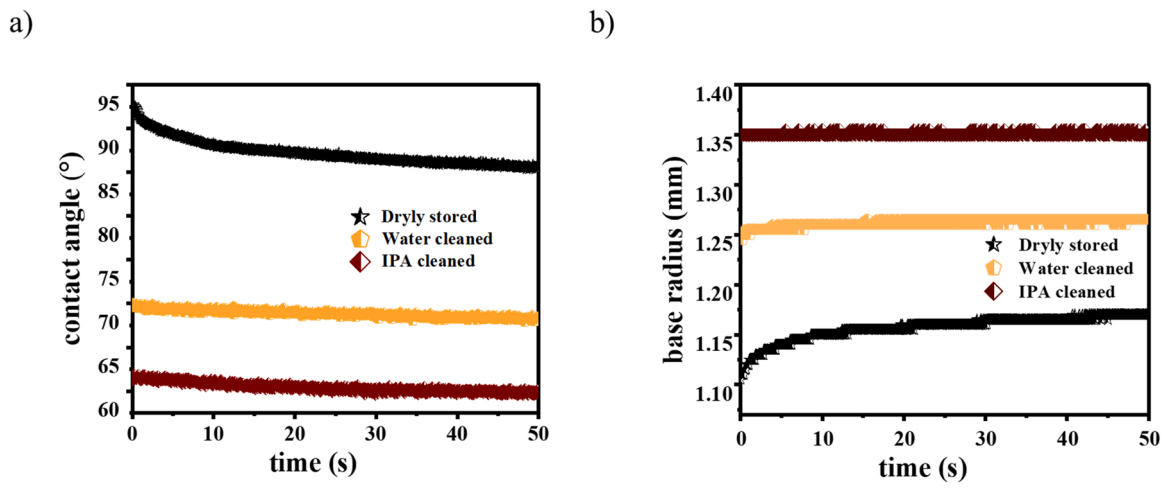

Fig. 8. (a) Decrease in the contact angle for pretreated surfaces compared to a dryly stored surface (negative side); (b) Evolution of the base radius (spreading) of a droplet deposited on the pretreated surfaces. Steps in the curves (corresponding to the spatial resolution of the images) occur because the increase in radius itself is small compared to the absolute droplet diameter.

water layers always exist on LN surfaces [73]. Also Atomic Force Microscopy based imaging on LN z-cut has shown adsorption of various species [47]. As discussed above, purposely letting water or isopropanol adsorb to the surface, significantly changes both the spreading time as well as the absolute contact angle. In addition to this, it has been shown that the polarization direction of the LN surface also influences the adsorption layer thickness and the adsorbing species [73]. X-ray Photoelectron Spectroscopy (XPS) studies on LN z-cut surfaces demonstrated higher water affinity on $+z$-cut surface as compared to the $-z$-cut [73]. It is also likely that the different thickness of adsorption layers on the oppositely poled faces of the LN wafer lead to different contact angles. In our experiments, we found that the contact angle is lower on $+z$-cut than on the $-z$-cut. This seems to go in line with the higher water affinity on the positive side. In general, adsorption processes and electric surface charges are inherently coupled.

If we assume an adsorption layer or a layer of charges to be present on the surface, deposition of a droplet will require the whole system to find to a new equilibrium, including the adsorbed layer.

For such a system, the initial state of the surface will depend on the environmental conditions, e.g. humidity of the air, previous cleaning processes, annealing etc. For example, there could be water, a different fluid, or various kinds of ions, dust, etc. adsorbed to the surface. Depending on the environmental conditions, adsorption could range from the presence of individual atoms over atomic layers to entire layers of liquid. XPS measurements reported a water layer thickness of about 0.5 – 1 nm, depending on the water vapor pressure [73]. In the case of a continuous water adsorption layer, there could also already be an electric double layer present at the surface (cp. Fig. 8(a) and (b), left side).

In general, an existing adsorption layer modifies both the "fluid-solid interface," i.e., the area beneath the droplet, as well as the "solid-gas interface," i.e., the area next to the droplet, when compared to a

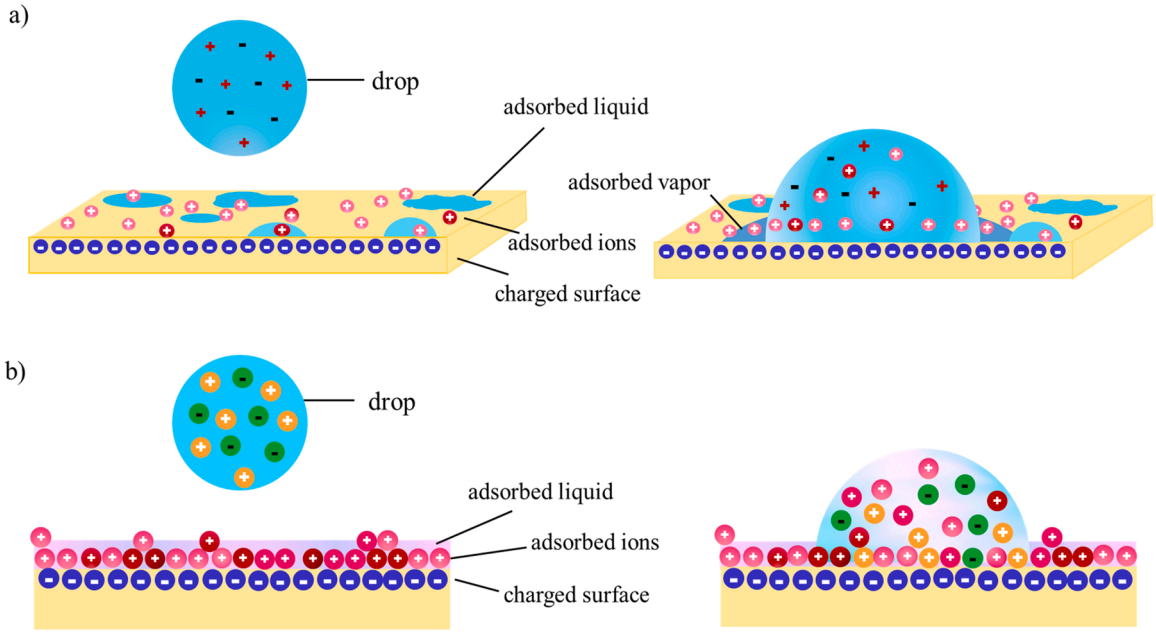

Fig. 9. Possible mechanisms taking place during the wetting of a charged surface: (a) Initial state with adsorbed moisture and ions or dust (left), illustration of possible vapor adsorption to the solid surface (right); (b) Initial state of an adsorbed liquid layer of the same or of a different fluid (left), illustration of possible rearrangement of adsorbed species underneath the droplet (right).

completely dry surface. Underneath the droplet, the droplet first only sees the adsorption layer instead of the solid surface. Next to the droplet, the surface energy also changes due to the presence of other species compared to a clean surface. Putting a droplet onto the surface will then require all contributing components to equilibrate, the "fluid-solid interface", the "solid-gas interface", as well as the bulk of the droplet.

Underneath the droplet, adsorbed species may become dissolved in the droplet, while ions from the droplet become adsorbed to the surface (cf. Fig. 9(b)). If initially, there is a water layer present, this could correspond to exchanging ions from the double layer or Stern layer. In the case of a layer of a different fluid being present (as after cleaning with isopropanol), mixing processes of the two fluids as well as possible Marangoni flows, could take place. In the case of dust adsorption, these substances could desorb from the surface and dissolve in the liquid droplet.

Since the surface is very susceptible to water adsorption, the presence of the droplet and its vapor may also change the adsorption of vapor from the gaseous environment next to the droplet. As the experiments on the contact angle evolution after cleaning showed, the surface needs several hours to attain its equilibrium with respect to adsorption. It is hence conceivable that similar equilibration processes also take place in the surroundings of the droplet, which could possibly lead to the large spreading time of the droplet (cf. Fig. 9(a)).

4. Conclusions

In this work, we investigated water-spreading dynamics on lithium niobate as an example of a widely employed ferroelectric material bearing a permanent surface charge. It, for the first time, provides studies of the dynamics of wetting on LN. It thereby shows the influence of intrinsic surface charges.

In our work, we found that the spreading dynamics differ from classic behavior. Spreading times on lithium niobate are strongly extended compared to classical wetting scenarios. Also, Tanner's law is not sufficient to describe the spreading dynamics on such material. Instead, an exponential spreading phase that follows Tanner's phase is dominating. While such a spreading phase should also be present for uncharged surfaces, it is usually not considered.

Furthermore, we found that an adsorbed layer of water or isopropanol significantly lowers the contact angle and speeds up the spreading process.

In any case, it is likely that adsorption layers play an important role in the wetting dynamic of lithium niobate, especially because the surface charge and moisture adsorption are inherently connected.

It is possible that the spreading properties observed for lithium niobate are similar in other charge-driven spreading processes, such as electrowetting. This especially applies to polymers, a widely used class of materials, because certain polymers can easily acquire surface charges. Also, insulator materials that acquire surface charges through an external electric field may be similar.

In addition, the large spreading times that were found during spreading may be important for the function and understanding of triboelectric nanogenerators and similar applications. They indicate that the time for a droplet to find to equilibrium (~minutes) is much larger than the contact time of a droplet with the surface in such applications (< 1 s).

In addition, the large influence of adsorption layers points out the significance of reproducible cleaning processes and storing conditions in wetting studies, especially with respect to charged surfaces.

Apart from this, solvent/liquid immersion-dependent wettability modifications might be exploited in ferroelectric-based device fabrication, such as sensors [39,40]. Polarization specific surface chemistries may provide a method for the fabrication of nanoscale devices [74] and in microfabrication [75] of electronics and high-density information storage devices. With all these properties, LN is an interesting material for developing nano- or microdroplet generators that aim to generate electrical energy from droplet motion. Furthermore, the polarization-specific surface chemistry of the material can be used in the understanding of surface charge-dependent cell interaction and the development of biocompatible material for tissue engineering [49,76].

Funding

The research initiative of the Rhineland-Palatinate is acknowledged for funding.

CRediT authorship contribution statement

Sushmitha Vinikumar: Conceptualization, Methodology, Investigation, Visualization, Writing. **Clarissa Schönecker:** Conceptualization, Supervision, Writing, Resources.

Declaration of Competing Interest

The authors declare that they have no known competing financial interests or personal relationships that could have appeared to influence the work reported in this paper.

Data availability

Data will be made available on request.

Acknowledgments

The authors thank Stefan Weber for pointing us to the material lithium niobate, and Aaron Ratschow for a stimulating discussion.

References

[1] M. Singh, H.M. Haverinen, P. Dhagat, G.E. Jabbour, Inkjet printing-process and its applications, Adv. Mater. 22 (2010) 673–685, https://doi.org/10.1002/adma.200901141.
[2] Z. Wang, D. Orejon, Y. Takata, K. Sefiane, Wetting and evaporation of multicomponent droplets, Phys. Rep. 960 (2022) 1–37, https://doi.org/10.1016/j.physrep.2022.02.005.
[3] B.J. Feenstra, R.A. Hayes, R. van Dijk, R. Boom, M. Wagemans, I. Camps, A. Giraldo, B. Heijden, Electrowetting-Based Displays: Bringing Microfluidics Alive On-Screen 48–53. https://doi.org/10.1109/MEMSYS.2006.1627733.
[4] G. Beni, M.A. Tenan, Dynamics of electrowetting displays, J. Appl. Phys. 52 (1981) 6011–6015, https://doi.org/10.1063/1.329822.
[5] D. Wang, Q. Sun, M.J. Hokkanen, C. Zhang, F.-Y. Lin, Q. Liu, S.-P. Zhu, T. Zhou, Q. Chang, B. He, Q. Zhou, L. Chen, Z. Wang, R.H.A. Ras, X. Deng, Design of robust superhydrophobic surfaces, Nature 582 (2020) 55–59, https://doi.org/10.1038/s41586-020-2331-8.
[6] S. Maheshwari, Y. Li, N. Agrawal, M.J. Janik, Density functional theory models for electrocatalytic reactions, in: C. Song (Ed.), Advances in Catalysis, Academic Press, Amsterdam, 2018, pp. 117–167.
[7] Y. Liang, Y. Han, J. Li, J. Wang, D. Liu, Q. Fan, Wettability control in electrocatalyst: A mini review, J. Energy Chem. (2021), https://doi.org/10.1016/j.jechem.2021.09.005.
[8] F. Mugele, J.-C. Baret, Electrowetting: from basics to applications, J. Phys.: Condens. Matter 17 (2005) R705–R774, https://doi.org/10.1088/0953-8984/17/28/R01.
[9] V. Srinivasan, V.K. Pamula, R.B. Fair, An integrated digital microfluidic lab-on-a-chip for clinical diagnostics on human physiological fluids, Lab Chip 4 (2004) 310–315, https://doi.org/10.1039/b403341h.
[10] M.G. Pollack, A.D. Shenderov, R.B. Fair, Electrowetting-based actuation of droplets for integrated microfluidics, Lab Chip 2 (2002) 96–101, https://doi.org/10.1039/b110474h.
[11] S.C. Jakeway, A.J. de Mello, E.L. Russell, Miniaturized total analysis systems for biological analysis, Fresenius, J. Anal. Chem. 366 (2000) 525–539, https://doi.org/10.1007/s002160051548.
[12] F.R. Smith, D. Brutin, Wetting and spreading of human blood: Recent advances and applications, Curr. Opin. Colloid Interface Sci. 36 (2018) 78–83, https://doi.org/10.1016/j.cocis.2018.01.013.
[13] O. Ghazian, K. Adamiak, G. Castle, Spreading and retraction control of charged dielectric droplets, Colloids Surf. A: Physicochem. Eng. Asp. 448 (2014) 23–33, https://doi.org/10.1016/j.colsurfa.2014.02.013.
[14] X. Zhang, L. Chen, Y. Jiang, W. Lim, S. Soh, Rationalizing the Triboelectric Series of Polymers, Chem. Mater. 31 (2019) 1473–1478, https://doi.org/10.1021/acs.chemmater.8b04526.

[15] A. Chen, C. Zhang, G. Zhu, Z.L. Wang, Polymer Materials for High-Performance Triboelectric Nanogenerators, Adv. Sci. (Weinh.) 7 (2020), 2000186, https://doi.org/10.1002/advs.202000186.
[16] R.E. Collins, Distribution of charge in electrets, Appl. Phys. Lett. 26 (1975) 675–677, https://doi.org/10.1063/1.88032.
[17] F. Johann, E. Soergel, Quantitative measurement of the surface charge density, Appl. Phys. Lett. 95 (2009), 232906, https://doi.org/10.1063/1.3269606.
[18] D.J. Lacks, T. Shinbrot, Long-standing and unresolved issues in triboelectric charging, Nat. Rev. Chem. 3 (2019) 465–476, https://doi.org/10.1038/s41570-019-0115-1.
[19] S.L. Burkett, E.M. Charlson, E.J. Charlson, H.K. Yasuda, Duck-Joo Yang, "The effect of cleaning procedures on surface charging of various substrates 8 (1995) 10–16.
[20] R. Manyala, Energy Harvesting, IntechOpen,, London, United Kingdom, 2018.
[21] T. Cheng, J. Shao, Z.L. Wang, Triboelectric nanogenerators, Nat. Rev. Methods Prim. 3 (2023) 1–13, https://doi.org/10.1038/s43586-023-00220-3.
[22] A.Z. Stetten, D.S. Golovko, S.A.L. Weber, H.-J. Butt, Slide electrification: charging of surfaces by moving water drops, Soft Matter 15 (2019) 8667–8679, https://doi.org/10.1039/c9sm01348b.
[23] S.-B. Jeon, D. Kim, G.-W. Yoon, J.-B. Yoon, Y.-K. Choi, Self-cleaning hybrid energy harvester to generate power from raindrop and sunlight, Nano Energy 12 (2015) 636–645, https://doi.org/10.1016/j.nanoen.2015.01.039.
[24] X. Li, P. Bista, A.Z. Stetten, H. Bonart, M.T. Schür, S. Hardt, F. Bodziony, H. Marschall, A. Saal, X. Deng, R. Berger, S.A.L. Weber, H.-J. Butt, Spontaneous charging affects the motion of sliding drops, Nat. Phys. 18 (2022) 713–719, https://doi.org/10.1038/s41567-022-01563-6.
[25] T. Krupenkin, J.A. Taylor, Reverse electrowetting as a new approach to high-power energy harvesting, Nat. Commun. 2 (2011) 448, https://doi.org/10.1038/ncomms1454.
[26] Z. Yang, E. Halvorsen, T. Dong, Power generation from conductive droplet sliding on electret film, Appl. Phys. Lett. 100 (2012), 213905, https://doi.org/10.1063/1.4720517.
[27] W. Xu, H. Zheng, Y. Liu, X. Zhou, C. Zhang, Y. Song, X. Deng, M. Leung, Z. Yang, R. X. Xu, Z.L. Wang, X.C. Zeng, Z. Wang, A droplet-based electricity generator with high instantaneous power density, Nature 578 (2020) 392–396, https://doi.org/10.1038/s41586-020-1985-6.
[28] Z.-H. Lin, G. Cheng, L. Lin, S. Lee, Z.L. Wang, Water-solid surface contact electrification and its use for harvesting liquid-wave energy, Angew. Chem. Int. Ed. Engl. 52 (2013) 12545–12549, https://doi.org/10.1002/anie.201307249.
[29] L.E. Helseth, Electrical energy harvesting from water droplets passing a hydrophobic polymer with a metal film on its back side, J. Electrost. 81 (2016) 64–70, https://doi.org/10.1016/j.elstat.2016.03.006.
[30] L.E. Helseth, X.D. Guo, Contact electrification and energy harvesting using periodically contacted and squeezed water droplets, Langmuir 31 (2015) 3269–3276, https://doi.org/10.1021/la503494c.
[31] S. Sinha, V. Padia, K.I. Bae, G. Chen, S. Das, Effect of electric double layer on electro-spreading dynamics of electrolyte drops, Colloids Surf. A: Physicochem. Eng. Asp. 514 (2017) 209–217, https://doi.org/10.1016/j.colsurfa.2016.11.031.
[32] W. Yan, D. Zhao, L. Zhang, R. Jia, N. Gao, D. Zhang, W. Luo, Y. Li, D. Liu, Optically induced reversible wettability transition on single crystal lithium niobate surfaces, Appl. Phys. Lett. 111 (2017) 91603, https://doi.org/10.1063/1.4995637.
[33] B. Tang, Y. Zhao, S. Yang, Z. Guo, Z. Wang, An Xing, X. Liu, Effect of surface charge characteristics of ferroelectric LiNbO3 on wettability of ionic liquids, Nanomater. (Basel) 12 (2022), https://doi.org/10.3390/nano12122085.
[34] R.M. Al-Shammari, M. Manzo, K. Gallo, J.H. Rice, B.J. Rodriguez, Tunable wettability of ferroelectric lithium niobate surfaces: the role of engineered microstructure and tailored metallic nanostructures, J. Phys. Chem. C. 121 (2017) 6643–6649, https://doi.org/10.1021/acs.jpcc.6b12336.
[35] D. Sun, Y. Zhang, D. Wang, W. Song, X. Liu, J. Pang, D. Geng, Y. Sang, H. Liu, Microstructure and domain engineering of lithium niobate crystal films for integrated photonic applications, Light Sci. Appl. 9 (2020) 197, https://doi.org/10.1038/s41377-020-00434-0.
[36] N.L.V. Carreno, V.G. Deon, R.M. Silva, L.R. Santana, R.M. Pereira, M.O. Orlandi, W. M. Ventura, A. Dias, J.G. Taylor, H.V. Fajardo, M.F. Mesko, Feasible and Clean Solid-Phase Synthesis of LiNbO 3 by Microwave-Induced Combustion and Its Application as Catalyst for Low-Temperature Aniline Oxidation, ACS Sustain. Chem. Eng. 6 (2018) 1680–1691, https://doi.org/10.1021/acssuschemeng.7b02921.
[37] Q. Fan, L. Lei, Y. Sun, Facile synthesis of a 3D-porous LiNbO3 nanocomposite as a novel electrode material for lithium ion batteries, Nanoscale 6 (2014) 7188–7192, https://doi.org/10.1039/c4nr00232f.
[38] A. Weiss, C. Frydendahl, J. Bar-David, R. Zektzer, E. Edrei, J. Engelberg, N. Mazurski, B. Desiatov, U. Levy, Tunable Metasurface Using Thin-Film Lithium Niobate in the Telecom Regime, ACS Photonics 9 (2022) 605–612, https://doi.org/10.1021/acsphotonics.1c01582.
[39] R.-C. Twu, H.-Y. Hou, Y.-H. Lee, Lithium niobate optical sensing chip for portable instrument, in: 2010 International Symposium on Micro-Nanomechatronics and Human Science, Nagoya, Japan, IEEE, Piscataway, NJ, 2010, pp. 252–257.
[40] J.P. Mathur, Optical Characterization Techniques for High-performance Microelectronic Device Manufacturing: 20 October 1994, SPIE, Bellingham, Wash.,, Austin, Texas, 1994.
[41] K. Luke, P. Kharel, C. Reimer, L. He, M. Loncar, M. Zhang, Wafer-scale low-loss lithium niobate photonic integrated circuits, Opt. Express 28 (2020) 24452–24458, https://doi.org/10.1364/OE.401959.
[42] D.L. Polla, L.F. Francis, Processing and characterization of piezoelectric materials and integration into microelectromechanical systems, Annu. Rev. Mater. Sci. 28 (1998) 563–597, https://doi.org/10.1146/annurev.matsci.28.1.563.
[43] Z.G. Hu, F.W. Shi, Z.M. Huang, Y.N. Wu, G.S. Wang, J.H. Chu, Spectroscopic ellipsometry investigations of PLT ferroelectric thin films with various La concentrations in the mid-infrared spectral region, Appl. Phys. A 80 (2005) 841–846, https://doi.org/10.1007/s00339-003-2322-2.
[44] P. Muralt, Micromachined infrared detectors based on pyroelectric thin films, Rep. Prog. Phys. 64 (2001) 1339–1388, https://doi.org/10.1088/0034-4885/64/10/203.
[45] B.W. Olson, J.L. Skinner, C.D. Richards, R.F. Richards, D.F. Bahr, Optimization of Thermal Processing and Chemistry in the Fabrication of a PZT Based Mems Power Generator, MRS Proc. 718 (2002), https://doi.org/10.1557/PROC-718-D10.25.
[46] G. Bettella, R. Zamboni, G. Pozza, A. Zaltron, C. Montevecchi, M. Pierno, G. Mistura, C. Sada, L. Gauthier-Manuel, M. Chauvet, LiNbO3 integrated system for opto-microfluidic sensing, Sens. Actuators B: Chem. 282 (2019) 391–398, https://doi.org/10.1016/j.snb.2018.10.082.
[47] S. Sanna, S. Rode, R. Hölscher, S. Klassen, C. Marutschke, K. Kobayashi, H. Yamada, W.G. Schmidt, A. Kühnle, Charge compensation by long-period reconstruction in strongly polar lithium niobate surfaces, Phys. Rev. B 88 (2013), https://doi.org/10.1103/PhysRevB.88.115422.
[48] C. Yakopcic, S. Wang, W. Wang, E. Shin, J. Boeckl, G. Subramanyam, T.M. Taha, Filament formation in lithium niobate memristors supports neuromorphic programming capability, Neural Comput. Applic 30 (2018) 3773–3779, https://doi.org/10.1007/s00521-017-2958-z.
[49] S. Danti, B. Azimi, M. Candito, A. Fusco, M.S. Sorayani Bafqi, C. Ricci, M. Milazzo, C. Cristallini, M. Latifi, G. Donnarumma, L. Bruschini, A. Lazzeri, L. Astolfi, S. Berrettini, Lithium niobate nanoparticles as biofunctional interface material for inner ear devices, Biointerphases 15 (2020) 31004, https://doi.org/10.1116/6.0000067.
[50] M. Candito, E. Simoni, E. Gentilin, A. Martini, G. Marioni, S. Danti, L. Astolfi, Neuron Compatibility and Antioxidant Activity of Barium Titanate and Lithium Niobate Nanoparticles, Int. J. Mol. Sci. 23 (2022), https://doi.org/10.3390/ijms23031761.
[51] B. Mandracchia, O. Gennari, A. Bramanti, S. Grilli, P. Ferraro, Label-free quantification of the effects of lithium niobate polarization on cell adhesion via holographic microscopy, J. Biophotonics 11 (2018), e201700332, https://doi.org/10.1002/jbio.201700332.
[52] S. Sanna, W.G. Schmidt, Lithium niobate X -cut, Y -cut, and Z -cut surfaces from ab initio theory, Phys. Rev. B 81 (2010), 214116, https://doi.org/10.1103/PhysRevB.81.214116.
[53] H. Chen, Y. Xie, G. Zhang, H. Yu, A first-principles investigation of the stabilities and electronic properties of SrZrO3 (1 1 0) (1 × 1) polar terminations, J. Phys. Condens. Matter 26 (2014), 395002, https://doi.org/10.1088/0953-8984/26/39/395002.
[54] R. Hölscher, W.G. Schmidt, S. Sanna, Modeling LiNbO 3 Surfaces at Ambient Conditions, J. Phys. Chem. C. 118 (2014) 10213–10220, https://doi.org/10.1021/jp502936f.
[55] S. Sanna, W.G. Schmidt, LiNbO3 surfaces from a microscopic perspective, J. Phys. Condens. Matter 29 (2017), 413001, https://doi.org/10.1088/1361-648X/aa818d.
[56] S.V. Levchenko, A.M. Rappe, Influence of ferroelectric polarization on the equilibrium stoichiometry of lithium niobate (0001) surfaces, Phys. Rev. Lett. 100 (2008), 256101, https://doi.org/10.1103/PhysRevLett.100.256101.
[57] V. Pruneri, J. Webjörn, P. Russell, J. Barr, D.C. Hanna, Intracavity second harmonic generation of 0.532 μm in bulk periodically poled lithium niobate, Opt. Commun. 116 (1995) 159–162, https://doi.org/10.1016/0030-4018(95)00035-7.
[58] L.L. Pendergrass, Ferroelectric microdomain reversal at room temperature in lithium niobate, J. Appl. Phys. 62 (1987) 231–236, https://doi.org/10.1063/1.339186.
[59] I. Camlibel, Spontaneous Polarization Measurements in Several Ferroelectric Oxides Using a Pulsed-Field Method, J. Appl. Phys. 40 (1969) 1690–1693, https://doi.org/10.1063/1.1657832.
[60] A. Turygin, D. Alikin, Y. Alikin, V. Shur, The Formation of Self-Organized Domain Structures at Non-Polar Cuts of Lithium Niobate as a Result of Local Switching by an SPM Tip, Mater. (Basel) 10 (2017), https://doi.org/10.3390/ma10101143.
[61] X. Liang, Y. Yu, R. Liu, W. Liu, S. Shen, Flexoelectricity in periodically poled lithium niobate by PFM, J. Phys. D: Appl. Phys. 55 (2022), 335303, https://doi.org/10.1088/1361-6463/ac7265.
[62] J.R. Maguire, H. Waseem, R.G.P. McQuaid, A. Kumar, J.M. Gregg, C. Cochard, Imaging Ferroelectrics: Reinterpreting Charge Gradient Microscopy as Potential Gradient Microscopy, Adv. Elect. Mater. 8 (2022), 2101384, https://doi.org/10.1002/aelm.202101384.
[63] X. Liu, K. Kitamura, K. Terabe, Surface potential imaging of nanoscale LiNbO3 domains investigated by electrostatic force microscopy, Appl. Phys. Lett. 89 (2006), 132905, https://doi.org/10.1063/1.2358115.
[64] T. Nagata, T. Chikyow, K. Kitamura, Screening charge localization at LiNbO 3 surface with Schottky junction, Appl. Phys. Lett. 108 (2016), 171604, https://doi.org/10.1063/1.4947578.
[65] A.-M. Cazabat, How does a droplet spread? Contemp. Phys. 28 (1987) 347–364, https://doi.org/10.1080/00107518708224600.
[66] M.S. Agrawal, H.S. Gaikwad, P.K. Mondal, G. Biswas, Analysis and experiments on the spreading dynamics of a viscoelastic drop, Appl. Math. Model. 75 (2019) 201–209, https://doi.org/10.1016/j.apm.2019.05.015.
[67] M.J. de Ruijter, J. de Coninck, G. Oshanin, Droplet spreading: partial wetting regime revisited, Langmuir 15 (1999) 2209–2216, https://doi.org/10.1021/la971301y.
[68] M.J. de Ruijter, J. de Coninck, T.D. Blake, A. Clarke, A. Rankin, Contact angle relaxation during the spreading of partially wetting drops, Langmuir 13 (1997) 7293–7298, https://doi.org/10.1021/la970825v.

[69] Aljaž. Velikonja, Ekaterina Gongadze Veronika, Kralj Iglič, Aleš. Iglič, Charge dependent capacitance of stern layer and capacitance, Int. J. Electrochem. Sci. 9 (2014) 5885–5894.
[70] T. Nagy, D. Henderson, D. Boda, Simulation of an electrical double layer model with a low dielectric layer between the electrode and the electrolyte, J. Phys. Chem. B 115 (2011) 11409–11419, https://doi.org/10.1021/jp2063244.
[71] O. Duran-Avendaño, C. Ramírez-Martín, O. Téquita, D. Figueredo, N.J. Cavieles, Implementation of an Impedance Spectroscopy Equipment for the Measurement of Electrochemical Parameters, IJET 10 (2018) 1310–1320, https://doi.org/10.21817/ijet/2018/v10i5/181005039.
[72] T.B. Jones, On the Relationship of Dielectrophoresis and Electrowetting, Langmuir 18 (2002) 4437–4443, https://doi.org/10.1021/la025616b.
[73] K. Cordero-Edwards, L. Rodríguez, A. Calò, M.J. Esplandiu, V. Pérez-Dieste, C. Escudero, N. Domingo, A. Verdaguer, Water Affinity and Surface Charging at the z-Cut and y-Cut LiNbO 3 Surfaces: An Ambient Pressure X-ray Photoelectron Spectroscopy, Study, J. Phys. Chem. C. 120 (2016) 24048–24055, https://doi.org/10.1021/acs.jpcc.6b05465.
[74] D. Li, M.H. Zhao, J. Garra, A.M. Kolpak, A.M. Rappe, D.A. Bonnell, J.M. Vohs, Direct in situ determination of the polarization dependence of physisorption on ferroelectric surfaces, Nat. Mater. 7 (2008) 473–477, https://doi.org/10.1038/nmat2198.
[75] J. Tien, A. Terfort, G.M. Whitesides, Microfabrication through Electrostatic Self-Assembly, Langmuir 13 (1997) 5349–5355, https://doi.org/10.1021/la970454i.
[76] V. Marchesano, O. Gennari, L. Mecozzi, S. Grilli, P. Ferraro, Effects of Lithium Niobate Polarization on Cell Adhesion and Morphology, ACS Appl. Mater. Interfaces 7 (2015) 18113–18119, https://doi.org/10.1021/acsami.5b05340.

Glossary

LN: lithium niobate
RH: relative humidity,
IPA: Isopropanol,
PET: poly(ethylene terephthalate),
DBP: Di-n-butyl phthalate,
KPFM: Kelvin probe force microscopy,
TENG: triboelectric nanogenerator,
XPS: X-ray Photoelectron Spectroscopy